ACS OMEGA

http://pubs.acs.org/journal/acsodf

Article

Computational Mechanistic Study of L-Aspartate Oxidase by ONIOM Method

Ibrahim Yildiz*

Cite This: *ACS Omega* 2023, 8, 19963−19968

Read Online

ACCESS | Metrics & More | Article Recommendations | Supporting Information

ABSTRACT: L-Aspartate oxidase (Laspo) is responsible for the oxidation of L-aspartate into iminoaspartate using flavin as a cofactor. During this process flavin is reduced, and it can be reoxidized by either molecular oxygen or fumarate. The overall fold and the catalytic residues of Laspo are similar to succinate dehydrogenase and fumarate reductase. On the basis of deuterium kinetic isotope effects as well as other kinetic and structural data, it is proposed that the enzyme can catalyze the oxidation of L-aspartate through a mechanism similar to amino acid oxidases. It is suggested that a proton is removed from the α-amino group, while a hydride is transferred from C2 to flavin. It is also suggested that the hydride transfer is a rate-limiting step. However, there is still an ambiguity about the stepwise or concerted mechanism of hydride- and proton-transfer steps. In this study, we formulated some computational models to study the hydride-transfer mechanism using the crystal structure of *Escherichia coli* L-aspartate oxidase in complexes with succinate. The calculations involved our own N-layered integrated molecular orbital and molecular mechanics method, and we evaluated the geometry and energetics of the hydride/proton-transfer processes while probing the roles of active site residues. Based on the calculations, it is concluded that proton- and hydride-transfer steps are decoupled, and a stepwise mechanism might be operative as opposed to the concerted one.

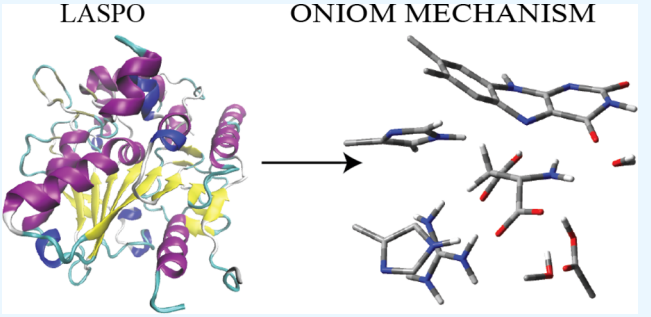

1. INTRODUCTION

Synthesis of NAD^+ is a crucial process for maintaining a number of cellular processes. In bacteria, synthesis of NAD^+ starts with the conversion of L-aspartate into iminoaspartate by L-aspartate oxidase (Laspo).[1] In the second step, iminoaspartate reacts with dihydroxyacetone phosphate, which is catalyzed by quinolinate synthase (NadA), to yield pyridine dicarboxylate, quinolinate. In the following steps, which are common to all organisms and not exclusive to bacteria, quinolinate is converted to NAD^+ through several enzymatic reactions.[2] Therefore, the first two steps could be utilized to design and develop drugs against some of the pathogenic bacteria.[3,4] Laspo is a member of flavoenzyme family, and the bound FAD cofactor oxidizes L-aspartate into iminoaspartate.[5] FAD can be reoxidized by either molecular oxygen to produce hydrogen peroxide under aerobic conditions or by fumarate under anaerobic conditions.

The crystal structure of Laspo derived from *Escherichia coli* shows that the folding topology of the enzyme is similar to the succinate dehydrogenase and fumarate reductase (SDH/FRD) family of oxidoreductases.[5] As a common feature, these enzymes act on dicarboxylic acid substrates.[6] Nonetheless, Laspo cannot oxidize succinate as compared to other similar reductases. Another marked difference is that Laspo oxidase has Glu121 in place of a neutral residue, which is present in other SDH/FRD family members.

Based on the similarities of Laspo to the SDH/FRD family, it was proposed that the oxidation of L-aspartate to iminoaspartate occurs through a mechanism similar to succinate oxidation (B in Figure 1). In this mechanism, the deprotonation of L-aspartate by an active site base at the C3 position is followed by the transfer of the hydride ion from C2 to FAD yielding iminoaspartate.[6] However, based on the oxidation mechanism of the other D-amino acid oxidases, this process may proceed through a different mechanism.[7,8] According to this mechanism, the α-amino group of aspartate is deprotonated by an active site base, and a hydride ion moves from C2 to FAD forming reduced FAD and iminoaspartate (A in Figure 1). Recently, Chow et al. reported a mechanistic study by performing primary solvent, multiple kinetic isotope effect, and primary kinetic isotope effect experiments for the aspartate oxidation half-reaction.[9] It was shown that the oxidation of L-aspartate by Laspo generated unlabeled malate in D_2O when malate dehydrogenase was present. It was concluded that the oxidation mechanism should

Received: March 23, 2023
Accepted: May 10, 2023
Published: May 25, 2023

https://doi.org/10.1021/acsomega.3c01949
ACS Omega 2023, 8, 19963−19968

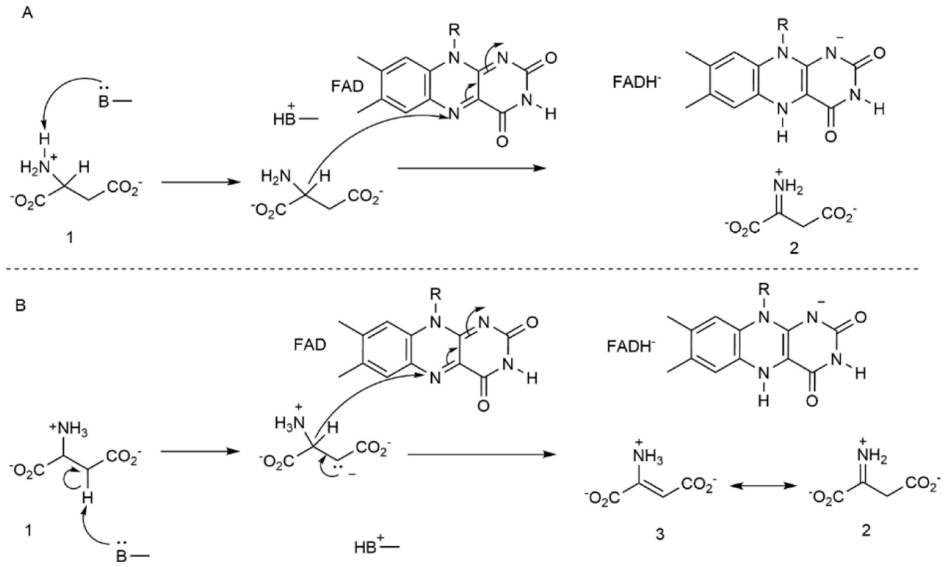

Figure 1. Oxidation of L-aspartate (1) into iminoaspartate (2) by Laspo through (A) concerted mechanism and (B) stepwise mechanism.

be similar to amino acid oxidases (A in Figure 1), and amine deprotonation and hydride-transfer steps might follow a concerted fashion rather than a stepwise.

The crystal structure of a mutant form of Laspo in complex with succinate (Figure 2) reveals important information about

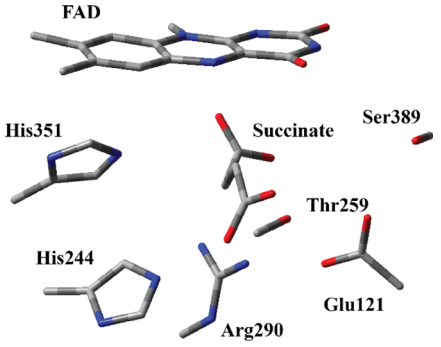

Figure 2. Structure of the active site of Laspo in complex with succinate including FAD and the surrounding residues.

the active site of the enyzme.[6] The isoalloxazine ring of FAD is in close proximity to succinate, which is surrounded by catalytically important residues, such as His244, His351, Thr259, Ser389, Glu121, and Arg290. It can be inferred that Glu121 is poised to act as the catalytic base, which can deprotonate the ammonium ion in the L-aspartate based on the mechanism proposed by Chow et al.[9] In addition, Arg290 and the other residues might have H-bonding interactions with the L-aspartate. The C2 position in succinate is in closed proximity to the N5 position of the isoalloxazine ring of FAD implying that hydride-ion transfer is likely to happen from the C2 position of L-aspartate.

Mechanistic studies of Laspo could provide invaluable insights in the design of novel therapeutics against bacterial infections. A number of experimental and computational studies favored the hydride-transfer mechanism for the oxidation of a variety of amines by flavin containing enzymes, such as D- and L-amino-acid oxidases, MAO-A and -B, and LHNO.[10−19] The solvent kinetic isotope effect study by Chow et al. showed that general base-catalyzed deprotonation of L-aspartate is a partially rate-determining process, and it rules out succinate dehydrogenase-like mechanisms (B in Figure 1) for L-aspartate.[9] In addition, due to the enamine−imine tautomerization process in this mechanism (3=>2 in B in Figure 1), the imine should incorporate a deuterium in D_2O if this mechanism is operative. NMR and ESI-MS studies did not show any deuterium incorporation. It was also suggested that hydride-transfer and proton-transfer steps should be concerted based on multiple kinetic isotope effects.

The hydride-transfer process for other enzymes, such as liver alcohol dehydrogenase,[20] aryl alcohol oxidase,[21,22] galactose oxidase,[23] HMG-CoA reductase,[24] and choline oxidase,[25] were studied computationally. Our own N-layered integrated molecular orbital and molecular mechanics (ONIOM) method, using quantum mechanics (QM) and molecular mechanics (MM) in the calculations, is an important tool to study mechanistic details of enzymatic reactions.[26−31] Density functional theory (DFT) calculations can highlight interactions and reactions involving substrates and active site residues, and the surrounding residues can be incorporated into model systems using molecular mechanics methods. By this way, a realistic 3-D model system reflecting the protein environment could be included in the calculations.

In this study, we studied the reaction mechanism of hydride transfer proposed by Chow et al. (A in Figure 1) for Laspo using the crystal structure of the enzyme−succinate complex with ONIOM method. The role of the active site residues was investigated using model geometries for enzyme−substrate complexes, transition states (TS), and enzyme−product complexes. We also highlighted the sequence of proton−hydride-transfer steps.

2. COMPUTATIONAL DETAILS AND METHODOLOGY

The model systems included two-layer ONIOM[27] calculations using three DFT functionals in the QM layer, including CAM-B3LYP,[32] M06-2X,[33] ωB97XD,[34] and AMBER force fields,[35] in the MM region using the Gaussian 09 package.[36] The CAM-B3LYP functional includes both the hybrid quality of B3LYP and long-range corrections;[26,37] the M06-2X functional yielded better results in comparison to B3LYP in the main-group chemistry;[38] ωB97XD provides empirical dispersion together with long-range corrections. RESP charges of each atom for

https://doi.org/10.1021/acsomega.3c01949
ACS Omega 2023, 8, 19963−19968

FAD and L-aspartate were calculated using HF/6-31G(d), and the missing MM parameters were derived using an antechamber option in AMBER 16.[39,40] Amber 94 MM charges were used for all atoms in the other residues. A mechanical embedding option was included in the calculations.

The geometries of the reactants, products, and TS were optimized using the 6-31G(d,p) basis set. TS are validated with the frequency calculations requiring one negative eigenvalue, and reactants and products were validated without any negative eigenvalues. Frequency calculations were done at 25 °C and 1 atm. TS structures were validated with intrinsic reaction coordinate (IRC) calculations.[41] TS structures were located through potential energy surface (PES) scans using scanning bond coordinates, and the maximum energy points in the scans were subjected to TS optimization using the Berny algorithm.[42]

ONIOM calculations used a truncated model enzyme, including FAD, L-aspartate, and the residues located around L-aspartate in a radius of 10 Å. The model enzyme-L-aspartate complex was obtained from the crystal structure of the succinate-bound enzyme (PDB accession code: 1KNP)[6] using the VMD program.[43] Succinate was converted to L-aspastate by attaching an ammonium group to the C2 position. This model consists of 1238 atoms, 96 residues, L-aspartate, and 2 water molecules. N-terminal and C-terminal residues on the periphery were capped with acetyl and N-methyl groups. This procedure not only mimics the electrostatic environment of the active site but also prevents creation of extra charged residues around the model active site, which might bring about considerable changes through strong chemical interactions. Protonation states of the residues with ionizable groups were determined using the PropKa program.[44] The total charge of ONIOM models was −3. In the ONIOM model system, the QM region included FAD, L-aspartate, and other catalytically important residues, such as His351, His244, Arg290, Thr259, Glu121, and Ser389, while the rest of the residues were placed in the MM region. The QM region included 95 atoms together with a total charge of −1. FAD and these residues were partitioned into QM and MM regions, and Figure 3 shows the QM region.

The initial model structure obtained from the crystal structure (Figure 2) together with L-aspartate was optimized using the M06-2X functional with a 6-31G(d,p) basis set to obtain an initial model enzyme−substrate-cofactor complex. A PES scan using the distance between the H atom at the C2 position of L-aspartate and N5 position of the FAD ring was performed to locate the TS structure for the hydride-transfer process (B in Figure 1). The geometry of the highest energy point in the PES scan was used optimized to locate the TS structure. The optimized structure of the reactant complex (RC) and product complex (PC) of the hydride-transfer process were obtained using proper geometries in the PES scan. RC and PC obtained with the PES scans were validated with the IRC calculation on the optimized TS structure.

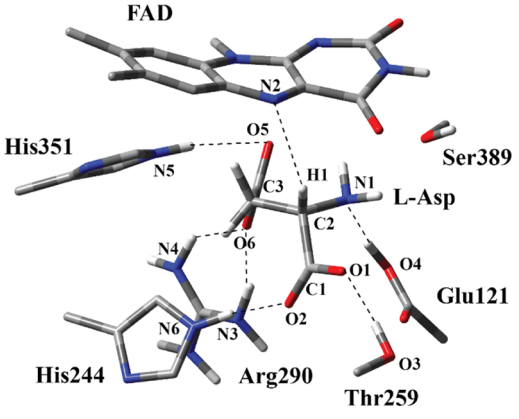

Figure 3. Structure of optimized RC, including FAD, L-aspatate, Glu121, His244, His351, Thr259, Arg290, and Ser389 in the QM region obtained with ONIOM [M06-2X/6-31G(d,p):Amber] with tube models. All the H atoms are excluded in the figure except the ones that belong to L-aspartate and others having H-bonding interactions.

3. RESULTS AND DISCUSSION

In this study, the proposed hydride-transfer mechanism for Laspo (A in Figure 1) was investigated using two-layer ONIOM (QM-MM) calculations. In this respect, the details of the hydride transfer were studied computationally, and the underlying non-covalent interactions together with the energetics of hydride-transfer process were highlighted. Besides, the proton-transfer process from the ammonium group of L-aspartate to a nearby basic residue is probed before and during the hydride-transfer process.

3.1. ONIOM Model Systems for Hydride-Transfer Mechanisms. *3.1.1. RC.* The optimized geometry of RC for the hydride-transfer process for the oxidation of L-aspartate into iminoaspartate reveals important mechanistic details (Figure 3). The ammonium group of L-aspartate is deprotonated by Glu121 indicating that Glu121 is the catalytic base for the proton-transfer step. Second, it shows that the proton-transfer step occurs before the hydride-transfer step. The initial calculation started with an un-optimized model structure in which L-aspartate contained ammonium cations and Glu121 had a negatively charged carboxylate anion. The optimization of this initial structure yielded a neutral amine group in L-asparate and protonated neutral Glu121. In order to locate a TS structure for the proton-transfer step between L-aspartate and Glu121 (N1 and O4 in Figure 3), a PES scan was performed on the optimized structure of RC (Figure 3). The distance between the proton on O4 in Glu 121 and N1 in L-aspartate was decreased in a number of steps. However, an uphill energy profile was obtained without a suitable candidate for the TS structure. This shows that the proton transfer from L-aspartate to Glu 121 is a barrier-less process. A series of H-bonding interactions between L-aspartate and surrounding residues holds L-aspartate close to the FAD's isoalloxazine ring. Because L-aspartate is a dicarboxylate anion, Arg290, His244, His351, and Thr259 have close H-bonding interactions, as shown with dotted lines in Figure 3. Protonated Glu121 has H-bonding interactions with amine N of L-aspartate (N1 in Figure 3). In addition, the isoalloxazine ring has a bent conformation, which is different from the succinate-bound crystal structure having planar conformation (Figure 2). The transition from planar to bent conformation was previously reported in some flavoenzymes upon substrate binding.[45] CAM-B3LYP and ωB97XD functionals produced similar RC structures as M062X.

3.1.2. TS. To be able to find a suitable TS structure candidate for the hydride-transfer process from L-aspartate to FAD, a relaxed PES scan was carried out by scanning the distance between the H atom at the C2 position of L-asparte (H1 in Figure 3) and the nitrogen atom at FAD (N2 in Figure 3). The highest energy point in the scan was subjected TS optimization. The resulting TS structure (Figure 4) shows that a hydride ion (H1 in Figure 4) is in departure from the C2 position of L-aspartate to the N2 position of FAD. Similar H-bonding

https://doi.org/10.1021/acsomega.3c01949
ACS Omega 2023, 8, 19963−19968

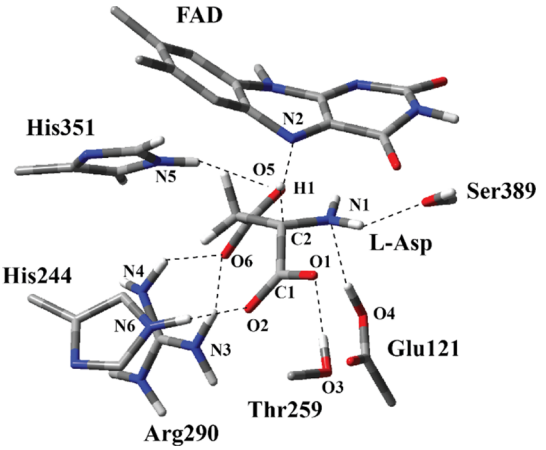

Figure 4. Structure of optimized TS including FAD, L-aspatate, Glu121, His244, His351, Thr259, Arg290, and Ser389 in the QM region obtained with ONIOM [M06-2X/6-31G(d,p):Amber] with tube models. All the H atoms are excluded in the figure except the ones that belong to L-aspartate and others having H-bonding interactions.

interactions as in the case of RC, shown as a dotted line, shows important H-bonding interactions. Arg290 has two H-bonding interactions with one of the O atoms of the carboxylate group of L-aspartate. (O6 in Figure 4). His351 interacts with the other O atom (O5 in Figure 4). The other carboxylate group in L-aspartate has H-bonding interactions with His244 and Thr259 (O1 and O2 in Figure 4). The H atom connected to O4 in Glu121 has a close H-bonding interaction with the amine N of L-aspartate (N1 in Figure 4). Furthermore, Ser389 interacts with L-aspartate. Another visible observation in the TS structure is that the bending of isoalloxazine ring is more prominent as compared to the RC structure (Figure 3). As the hydride anion (H1 in Figure 4) moves away from C2, C2 and N1 start to assume sp^2 characteristics and the bond distance shortens between them. CAM-B3LYP and ωB97XD functionals produced similar TS structures as M062X.

The Gibbs free energy difference between TS and RC, which is the activation energy for the hydride-transfer process (E_{af}) in terms of ONIOM energy, was calculated to be 24.37 kcal/mol with M062X functionals with the 6-31G(d,p) basis set in the QM region (E_{af}, at entry #1 in Table 1). This value was estimated closely with ωB97XD functionals. However, CAM-B3LYP estimated around 10 kcal/mol more energy barrier with respect to M062X and ωB97XD functionals. Based on the reported *k*cat value of the native enzyme for L-aspartate (40.0 ± 2.4 min^{-1}),[4] considering that the hydride transfer is the rate-limiting step, an activation barrier around 17−18 kcal/mol might be expected. Therefore, M062X and ωB97XD functionals estimate barriers closer to the expected range. Furthermore, activation energies based on ωB97XD and M062X results are closer to some reported calculated activation barriers for MAO and other oxidases for the hydride-transfer mechanism.[16,46,47] The activation energies of hydride-transfer process in terms of electronic energy were estimated to be 3−4 kcal more than the activation energies in terms of Gibbs free energy for three functionals (* values in Table 1). The activation energies of hydride-transfer process in terms of electronic energy were also calculated using single-point energy calculations with a larger basis set, 6-311 + G(2d,2p) for three functionals (** values in Table 1). 6-311 + G(2d,2p) basis sets produced 1−2 kcal/mol more activation energies than 6-31G(d,p) basis sets. It is observed enthalpic and entropic contributions to the Gibbs free energy together with zero-point energy correction lowers the activation barrier. An initial molecular dynamics simulation on the enzyme−substrate complex could provide a better initial model system for the calculations, which might further produce more accurate energy barriers.

3.1.3. PC. The optimized the geometry of PC (Figure 5) for the hydride-transfer process corresponds to the reduced

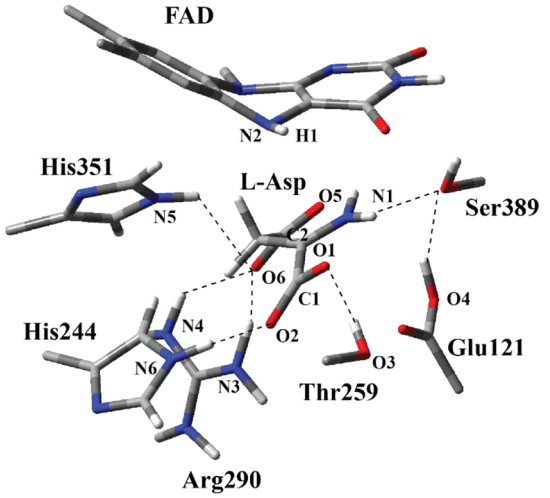

Figure 5. Structure of optimized PC, including FAD, L-aspatate, Glu121, His244, His351, Thr259, Arg290, and Ser389 in the QM region obtained with ONIOM [M06-2X/6-31G(d,p):Amber] with tube models. All the H atoms are excluded in the figure except the ones that belong to L-aspartate and others having H-bonding interactions.

isoalloxazine and iminium intermediate. The hydride ion completely transferred to the N2 position of isoalloxazine ring forming reduced FAD. L-aspartate is converted to an iminium ion having a planar geometry around the C2 position. Isoalloxazine ring conformation is considerably bent with a nearly 45° angle between benzene and pyrimidine groups.

Table 1. Energy Profile for the Hydride-Transfer Process for ONIOM Calculations Using CAM-B3LYP, M062X, and ωB97XD Functionals in the QM Region with 6-31G(d,p) Basis Sets[a]

entry #	functional	Ea_f (kcal/mol)	Ea_r (kcal/mol)	imaginary frequency (i)
1	M062X	24.37, 28.05*, 29.46**	34.73, 33.57*, 35.81**	−1281.76
2	ωB97XD	24.17, 26.80*, 28.46**	35.13, 33.57*, 37.95*	−1287.75
3	CAM-B3LYP	34.95, 37.62*, 38.08**	37.39, 36.26*, 40.97**	−1401.88

[a](E_{af}: activation energy for the forward reaction in kcal/mol in terms of ONIOM Gibbs free energy, E_{ar}: activation energy for the reverse reaction in kcal/mol in terms of ONIOM Gibbs free energy). The activation energy values with * refers to activation energies in terms of ONIOM electronic energy obtained with 6-31G(d,p) basis set, and ** refers to activation energies in terms of ONIOM electronic energy obtained with 6-311 + G(2d,2p) basis set through single point energy calculations.

https://doi.org/10.1021/acsomega.3c01949
ACS Omega 2023, 8, 19963−19968

Similar H-bonding interactions exist as in the case of TS. Glu121 has H-bonding interactions with Ser389, which interacts with N1 of iminium intermediate. His351 interacts with one of the carboxylate O atom in L-aspartate (O6 in Figure 5). In TS and RC structures (Figures 3 and 4), His351 interacts with the other carboxylate O atom (O5). CAM-B3LYP and ωB97XD functionals produced similar PC structures to M062X.

The Gibbs free energy difference between TS and PC, which is the activation energy for the reverse hydride-transfer process (E_{ar}) in terms of ONIOM energy, was calculated around to be 34−37 kcal/mol with three functionals (Table 1). This indicates that hydride transfer is an exergonic process. PC is stabilized by H-bonding interactions more than the RC structure. M062X and ωB97XD functionals estimated less barriers for the reverse process. 6-311 + G(2d,2p) basis set produced 2−4 kcal/mol more activation energies than the 6-31G(d,p) basis set in terms of electronic energy for the reverse hydride-transfer process for three functionals.

4. CONCLUSIONS

In this study, computational models using hybrid QM-MM calculations were formulated to analyze the hydride-transfer mechanism for the oxidation of L-aspartate by Laspo into iminium intermediates and reduced FAD. Using PES scans, a productive enzyme-cofactor-substrate RC, TS, and PC were generated using the available crystal structure of the enzyme. These models highlighted the roles of active site residues during the hydride-transfer process from the substrate to the isoalloxazine ring. It was found that a series of H-bonding interactions between FAD and the substrate keep them closer. Most importantly, Glu121 acts as the catalytic base for the proton-transfer step, and this step occurs prior to the hydride-transfer process without a barrier. ONIOM calculations revealed a bent FAD conformation before, during, and after hydride-transfer processes. Our models provide insights for the oxidation of L-aspartate by Laspo. These results may be used to study further details of the enzyme mechanism. In future, molecular dynamics studies can be coupled with QM-MM studies to elucidate more mechanistic insights into the oxidation of L-aspartate by Laspo.

■ ASSOCIATED CONTENT

Supporting Information

The Supporting Information is available free of charge at https://pubs.acs.org/doi/10.1021/acsomega.3c01949.

Gibbs free energy, enthalpy, and zero-point corrected electronic energies of RC, TS, and PC structures with three different DFT functionals (PDF)

Gaussian input files for optimized RC, TS, and PC structures with M062X functionals (ZIP)

■ AUTHOR INFORMATION

Corresponding Author

Ibrahim Yildiz − *Chemistry Department, Khalifa University, 127788 Abu Dhabi, UAE;* orcid.org/0000-0003-3321-0306; Phone: +971 (0)2 401 8208; Email: ibrahim.yildiz@ku.ac.ae

Complete contact information is available at: https://pubs.acs.org/10.1021/acsomega.3c01949

Notes

The author declares no competing financial interest.

■ ACKNOWLEDGMENTS

The authors acknowledge the contribution of High-Performance Computing Facility and Applied Material Chemistry Center (AMCC) at Khalifa University.

■ REFERENCES

(1) Magni, G.; Amici, A.; Emanuelli, M.; Raffaelli, N.; Ruggieri, S., Enzymology of Nad(+) Synthesis. *Advances in Enzymology*; Elsevier, Vol 73 1999, pp 135.

(2) Gazzaniga, F.; Stebbins, R.; Chang, S. Z.; McPeek, M. A.; Brenner, C. Microbial Nad Metabolism: Lessons from Comparative Genomics. *Microbiology and Molecular Biology Reviews* **2009**, *73*, 529−541.

(3) Tedeschi, G.; Negri, A.; Mortarino, M.; Ceciliani, F.; Simonic, T.; Faotto, L.; Ronchi, S. l-Aspartate Oxidase from Escherichia coli. II. Interaction with C4 Dicarboxylic Acids and Identification of a Novel l-Aspartate:Fumarate Oxidoreductase Activity. *Eur. J. Biochem.* **1996**, *239*, 427−433.

(4) Tedeschi, G.; Nonnis, S.; Strumbo, B.; Cruciani, G.; Carosati, E.; Negri, A. On the Catalytic Role of the Active Site Residue E121 of E. Coli L-Aspartate Oxidase. *Biochimie* **2010**, *92*, 1335−1342.

(5) Mattevi, A.; Tedeschi, G.; Bacchella, L.; Coda, A.; Negri, A.; Ronchi, S. Structure of L-Aspartate Oxidase: Implications for the Succinate Dehydrogenase/Fumarate Reductase Oxidoreductase Family. *Structure* **1999**, *7*, 745−756.

(6) Bossi, R. T.; Negri, A.; Tedeschi, G.; Mattevi, A. Structure of Fad-Bound L-Aspartate Oxidase: Insight into Substrate Specificity and Catalysis. *Biochemistry* **2002**, *41*, 3018−3024.

(7) Hersh, L. B.; Jorns, M. S. Use of 5-Deazafad to Study Hydrogen Transfer in the D-Amino Acid Oxidase Reaction. *The Journal of biological chemistry* **1975**, *250*, 8728−8734.

(8) Miura, R.; Miyake, Y. The Reaction-Mechanism of D-Amino-Acid Oxidase - Concerted or Not Concerted. *Bioorg. Chem.* **1988**, *16*, 97−110.

(9) Chow, C.; Hegde, S.; Blanchard, J. S. Mechanistic Characterization of *Escherichia coli* l-Aspartate Oxidase from Kinetic Isotope Effects. *Biochemistry* **2017**, *56*, 4044−4052.

(10) Fitzpatrick, P. F. Carbanion Versus Hydride Transfer Mechanisms in Flavoprotein-Catalyzed Dehydrogenations. *Bioorg. Chem.* **2004**, *32*, 125−139.

(11) Harris, C. M.; Pollegioni, L.; Ghisla, S. Ph and Kinetic Isotope Effects in D-Amino Acid Oxidase Catalysis. *Eur. J. Biochem.* **2001**, *268*, 5504−5520.

(12) Atalay, V. E.; Erdem, S. S. A Comparative Computational Investigation on the Proton and Hydride Transfer Mechanisms of Monoamine Oxidase Using Model Molecules. *Comput. Biol. Chem.* **2013**, *47*, 181−191.

(13) Cakir, K.; Erdem, S. S.; Atalay, V. E. Oniom Calculations on Serotonin Degradation by Monoamine Oxidase B: Insight into the Oxidation Mechanism and Covalent Reversible Inhibition. *Organic & biomolecular chemistry* **2016**, *14*, 9239−9252.

(14) Kachalova, G. S.; Bourenkov, G. P.; Mengesdorf, T.; Schenk, S.; Maun, H. R.; Burghammer, M.; Riekel, C.; Decker, K.; Bartunik, H. D. Crystal Structure Analysis of Free and Substrate-Bound 6-Hydroxy-L-Nicotine Oxidase from Arthrobacter Nicotinovorans. *J. Mol. Biol.* **2010**, *396*, 785−799.

(15) Pawelek, P. D.; Cheah, J.; Coulombe, R.; Macheroux, P.; Ghisla, S.; Vrielink, A. The Structure of L-Amino Acid Oxidase Reveals the Substrate Trajectory into an Enantiomerically Conserved Active Site. *The EMBO Journal* **2000**, *19*, 4204−4215.

(16) Akyüz, M. A.; Erdem, S. S. Computational Modeling of the Direct Hydride Transfer Mechanism for the Mao Catalyzed Oxidation of Phenethylamine and Benzylamine: Oniom (Qm/Qm) Calculations. *Journal of Neural Transmission* **2013**, *120*, 937−945.

(17) Brela, M. Z.; Prah, A.; Boczar, M.; Stare, J.; Mavri, J. Path Integral Calculation of the Hydrogen/Deuterium Kinetic Isotope Effect in Monoamine Oxidase a-Catalyzed Decomposition of Benzylamine. *Molecules* **2019**, *24*, 4359.

(18) Zapata-Torres, G.; Fierro, A.; Barriga-González, G.; Salgado, J. C.; Celis-Barros, C. Revealing Monoamine Oxidase B Catalytic Mechanisms by Means of the Quantum Chemical Cluster Approach. *J. Chem. Inf. Model.* **2015**, *55*, 1349−1360.
(19) Vianello, R.; Domene, C.; Mavri, J. The Use of Multiscale Molecular Simulations in Understanding a Relationship between the Structure and Function of Biological Systems of the Brain: The Application to Monoamine Oxidase Enzymes. *Frontiers in Neuroscience* **2016**, *10*, DOI: 10.3389/fnins.2016.00327.
(20) Agarwal, P. K.; Webb, S. P.; Hammes-Schiffer, S. Computational Studies of the Mechanism for Proton and Hydride Transfer in Liver Alcohol Dehydrogenase. *J. Am. Chem. Soc.* **2000**, *122*, 4803−4812.
(21) Hernández-Ortega, A.; Borrelli, K.; Ferreira, P.; Medina, M.; Martínez, A. T.; Guallar, V. Substrate Diffusion and Oxidation in Gmc Oxidoreductases: An Experimental and Computational Study on Fungal Aryl-Alcohol Oxidase. *Biochem. J.* **2011**, *436*, 341−350.
(22) Hernández-Ortega, A.; Ferreira, P.; Merino, P.; Medina, M.; Guallar, V.; Martínez, A. T. Stereoselective Hydride Transfer by Aryl-Alcohol Oxidase, a Member of the Gmc Superfamily. *ChemBioChem* **2012**, *13*, 427−435.
(23) Verma, P.; Pratt, R. C.; Storr, T.; Wasinger, E. C.; Stack, T. D. P. Sulfanyl Stabilization of Copper-Bonded Phenoxyls in Model Complexes and Galactose Oxidase. *Proc. Natl. Acad. Sci. U.S.A.* **2011**, *108*, 18600−18605.
(24) Haines, B. E.; Steussy, C. N.; Stauffacher, C. V.; Wiest, O. Molecular Modeling of the Reaction Pathway and Hydride Transfer Reactions of Hmg-Coa Reductase. *Biochemistry* **2012**, *51*, 7983−7995.
(25) Yildiz, I.; Yildiz, B. S.; Kirmizialtin, S. Comparative Computational Approach to Study Enzyme Reactions Using Qm and Qm-Mm Methods. *ACS Omega* **2018**, *3*, 14689−14703.
(26) Lonsdale, R.; Harvey, J. N.; Mulholland, A. J. A Practical Guide to Modelling Enzyme-Catalysed Reactions. *Chem. Soc. Rev.* **2012**, *41*, 3025−3038.
(27) Vreven, T.; Byun, K. S.; Komáromi, I.; Dapprich, S.; Montgomery, J. A.; Morokuma, K.; Frisch, M. J. Combining Quantum Mechanics Methods with Molecular Mechanics Methods in Oniom. *J. Chem. Theory Comput.* **2006**, *2*, 815−826.
(28) Chen, J.; Wang, J.; Zhang, Q.; Chen, K.; Zhu, W. Probing Origin of Binding Difference of Inhibitors to Mdm2 and Mdmx by Polarizable Molecular Dynamics Simulation and Qm/Mm-Gbsa Calculation. *Sci. Rep.* **2015**, *5*, 17421.
(29) Chen, J.; Wang, J.; Zhang, Q.; Chen, K.; Zhu, W. A Comparative Study of Trypsin Specificity Based on Qm/Mm Molecular Dynamics Simulation and Qm/Mm Gbsa Calculation. *Journal of Biomolecular Structure and Dynamics* **2015**, *33*, 2606−2618.
(30) Chung, L. W.; Sameera, W. M. C.; Ramozzi, R.; Page, A. J.; Hatanaka, M.; Petrova, G. P.; Harris, T. V.; Li, X.; Ke, Z.; Liu, F.; et al. The Oniom Method and Its Applications. *Chem. Rev.* **2015**, *115*, 5678−5796.
(31) Lundberg, M.; Morokuma, K., The Oniom Method and Its Applications to Enzymatic Reactions. In *Multi-Scale Quantum Models for Biocatalysis: Modern Techniques and Applications*, York; Lee, T.-S., Ed. Springer Netherlands: Dordrecht, 2009; pp 21-55.
(32) Yanai, T.; Tew, D. P.; Handy, N. C. A New Hybrid Exchange−Correlation Functional Using the Coulomb-Attenuating Method (Cam-B3lyp). *Chem. Phys. Lett.* **2004**, *393*, 51−57.
(33) Zhao, Y.; Truhlar, D. The M06 Suite of Density Functionals for Main Group Thermochemistry, Thermochemical Kinetics, Noncovalent Interactions, Excited States, and Transition Elements: Two New Functionals and Systematic Testing of Four M06-Class Functionals and 12 Other Functionals. *Theor Chem Account* **2008**, *120*, 215−241.
(34) Chai, J.-D.; Head-Gordon, M. Systematic Optimization of Long-Range Corrected Hybrid Density Functionals. *J. Chem. Phys.* **2008**, *128*, 084106.
(35) Hornak, V.; Abel, R.; Okur, A.; Strockbine, B.; Roitberg, A.; Simmerling, C. Comparison of Multiple Amber Force Fields and Development of Improved Protein Backbone Parameters. *Proteins* **2006**, *65*, 712−725.
(36) Frisch, M. J.; et al. *Gaussian 09*; Gaussian, Inc.: Wallingford, CT, USA, 2009.
(37) Meunier, B.; de Visser, S. P.; Shaik, S. Mechanism of Oxidation Reactions Catalyzed by Cytochrome P450 Enzymes. *Chem. Rev.* **2004**, *104*, 3947−3980.
(38) Zhao, Y.; Truhlar, D. G. Applications and Validations of the Minnesota Density Functionals. *Chem. Phys. Lett.* **2011**, *502*, 1−13.
(39) Cornell, W. D.; Cieplak, P.; Bayly, C. I.; Kollman, P. A. Application of Resp Charges to Calculate Conformational Energies, Hydrogen Bond Energies, and Free Energies of Solvation. *J. Am. Chem. Soc.* **1993**, *115*, 9620−9631.
(40) Case, D.; Berryman, J.; Betz, R.; Cerutti, D.; Cheatham, T., III; Darden, T.; Duke, R.; Giese, T.; Gohlke, H.; Goetz, A., *Amber 2015*; University of California: San Francisco, Ca, 2015. There is no corresponding record for this reference.[Google Scholar].
(41) Hratchian, H. P.; Schlegel, H. B. Chapter 10 - Finding Minima, Transition States, and Following Reaction Pathways on Ab Initio Potential Energy Surfaces A2 - Dykstra, Clifford E. In *Theory and Applications of Computational Chemistry*; Frenking, G., Kim, K. S., Scuseria, G. E., Eds.; Elsevier: Amsterdam, 2005, pp 195−249.
(42) Peng, C.; Ayala, P. Y.; Schlegel, H. B.; Frisch, M. J. Using Redundant Internal Coordinates to Optimize Equilibrium Geometries and Transition States. *J. Comput. Chem.* **1996**, *17*, 49−56.
(43) Humphrey, W.; Dalke, A.; Schulten, K. Vmd: Visual Molecular Dynamics. *Journal of Molecular Graphics* **1996**, *14*, 33−38.
(44) Davies, M. N.; Toseland, C. P.; Moss, D. S.; Flower, D. R. Benchmarking Pk(a) Prediction. *BMC Biochem* **2006**, *7*, 18.
(45) Lennon, B. W.; Williams, C. H., Jr.; Ludwig, M. L. Crystal Structure of Reduced Thioredoxin Reductase from Escherichia Coli: Structural Flexibility in the Isoalloxazine Ring of the Flavin Adenine Dinucleotide Cofactor. *Protein Sci.* **2008**, *8*, 2366−2379.
(46) Yu, L.-J.; Golden, E.; Chen, N.; Zhao, Y.; Vrielink, A.; Karton, A. Computational Insights for the Hydride Transfer and Distinctive Roles of Key Residues in Cholesterol Oxidase. *Sci. Rep.* **2017**, *7*, 17265.
(47) Erdem, S. S.; Büyükmenekşe, B. Computational Investigation on the Structure−Activity Relationship of the Biradical Mechanism for Monoamine Oxidase. *Journal of Neural Transmission* **2011**, *118*, 1021−1029.

https://doi.org/10.1021/acsomega.3c01949
ACS Omega 2023, 8, 19963−19968